ACS OMEGA

Article

http://pubs.acs.org/journal/acsodf

Zirconium Oxynitride-Catalyzed Oxygen Reduction Reaction at Polymer Electrolyte Fuel Cell Cathodes

Mitsuharu Chisaka,*[,†] Akimitsu Ishihara,[‡,§] Hiroyuki Morioka,[∥] Takaaki Nagai,[‡] Shihong Yin,[‡] Yoshiro Ohgi,[⊥] Koichi Matsuzawa,[‡] Shigenori Mitsushima,[‡,§] and Ken-ichiro Ota[‡]

[†]Department of Sustainable Energy, Hirosaki University, 3 Bunkyo-cho, Hirosaki, Aomori 036-8561, Japan

[‡]Green Hydrogen Research Center and [§]Institute of Advanced Sciences, Yokohama National University, 79-5 Tokiwadai, Hodogaya-ku, Yokohama, Kanagawa 240-8501, Japan

[∥]Technical Research Institute, Toppan Printing Co., Ltd, 4-2-3 Takanodaiminami, Sugito-machi, Saitama 345-8508, Japan

[⊥]Kumamoto Industrial Research Institute, 3-11-38 Azuma-cho, Azuma-ku, Kumamoto, Kumamoto 862-0901, Japan

Supporting Information

ABSTRACT: Most nonplatinum group metal (non-PGM) catalysts for polymer electrolyte fuel cell cathodes have so far been limited to iron(cobalt)/nitrogen/carbon [Fe(Co)/N/C] composites owing to their high activity in both half-cell and single-cell cathode processes. Group IV and V metal oxides, another class of non-PGM catalysts, are stable in acidic media; however, their activities have been mostly evaluated for half-cells, with no single-cell performances comparable to those of Fe/N/C composites reported to date. Herein, we report successful syntheses of zirconium oxynitride catalysts on multiwalled carbon nanotubes, which show the highest oxygen reduction reaction activity among oxide-based catalysts. The single-cell performance of these catalysts reached 10 mA cm^{-2} at 0.9 V, being comparable to that of state-of-the-art Fe/N/C catalysts. This new record opens up a new pathway for reaching the year 2020 target set by the U.S. Department of Energy, that is, 44 mA cm^{-2} at 0.9 V.

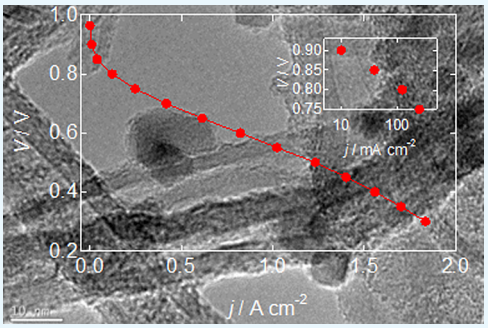

1. INTRODUCTION

The cathodic oxygen reduction reaction (ORR) is a rate-determining step in numerous fuel cells and air batteries, with the rate being particularly low for polymer electrolyte fuel cell (PEFC) cathodes because of their low operating temperature of ~353 K and the acidic environment (pH ≤ 1).[1] Therefore, a significant amount of platinum group metal (PGM) catalysts have been used for lowering the overpotential. Although PEFC-powered vehicles and stationary power generation units have been commercialized in the last decade, the usage of PGM catalysts is still too high for their widespread use.[2,3] The economic impact of vehicles motivated many researchers to develop non-PGM catalysts for PEFC cathodes; however, the acidic environment and the high operating potential of 0.6−1.0 V versus the reversible hydrogen electrode (RHE) limit the choice of non-PGM catalysts, with only two types extensively studied in the last decade. The first type corresponds to iron/cobalt, nitrogen, and carbon [Fe(Co)/N/C] catalysts, displaying high activity in both half-cells with acidic solutions and single cells.[3−14] These catalysts can be synthesized by one- or two-step pyrolysis of Fe(Co)/N/C sources to produce nitrogen-doped graphitic carbon materials, possessing at least three different active site types proposed to date: (1) iron/cobalt atoms coordinated by two or four nitrogen atoms located at the edge of graphitic carbon layers,[3−10] (2) nitrogen-doped carbon species,[5,11,12] and (3) iron carbide[13] or iron particles[14] encased in graphitic carbon layers. As type-2 active sites are present in type-1 sites, the discussion is sometimes controversial.[3] It is generally accepted that the presence of iron/cobalt species during pyrolysis is necessary to produce state-of-the-art highly active sites, with the onset potential falling below 0.8 V versus RHE, when such catalysts are synthesized in the absence of these species.[3]

Group IV and V metal oxides/oxynitrides are another class of non-PGM catalysts for PEFC cathodes. Catalysts of this type are resistant to leaching in acidic media, as confirmed by using inductively coupled plasma spectroscopy.[15−19] These catalysts were discovered in the mid-2000s, approximately 40 years after Jasinski's discovery of cobalt phthalocyanine,[20] which is the origin of today's Fe(Co)/N/C catalysts. Because of the short development period of oxide/oxynitride catalysts, their activity has mostly been evaluated by screening half-cells containing acidic solutions,[15−19,21−43] with the insulating nature of these species requiring much effort. For example, micron-sized zirconium oxide powders and carbon black were mechanically mixed, and then, the mass ratio and the type of carbon black were optimized to form a catalyst layer on a glassy carbon (GC) electrode.[21] Because such optimizations are time-consuming,

Received: December 27, 2016
Accepted: February 14, 2017
Published: February 23, 2017

DOI: 10.1021/acsomega.6b00555
ACS Omega 2017, 2, 678−684

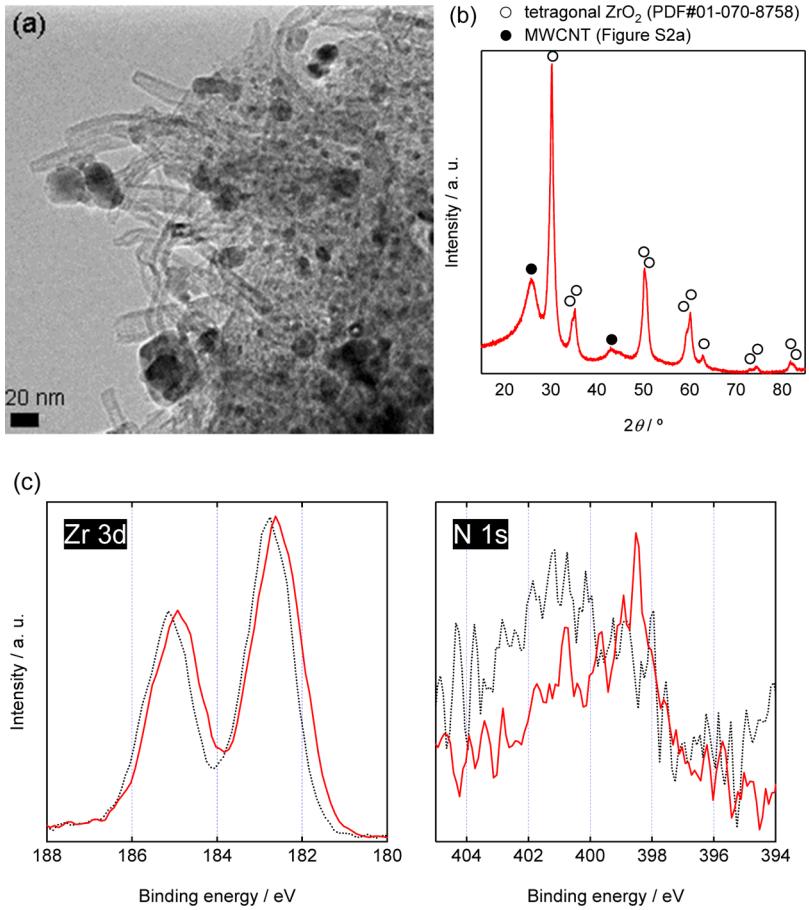

Figure 1. (a) TEM image, (b) XRD pattern, and (c) Zr 3d and N 1s spectra of the ZrO_xN_y–MWCNT catalyst after NH_3 pyrolysis at 973 K. For comparison, Zr 3d and N 1s spectra of ZrO_xN_y–MWCNTs before NH_3 pyrolysis are shown by dashed lines in (c).

recent studies have focused on the synthesis of nanoparticles on conductive carbon materials. Nanosized titanium oxynitride,[22−26] zirconium oxide,[27,28] zirconium oxynitride,[29] niobium oxide,[27,30] niobium oxynitride,[31] hafnium oxide,[32] hafnium oxynitride,[19,33−36] aluminum-doped hafnium oxynitride,[37] tantalum oxide,[27,38−41] sodium-doped tantalum oxide,[42] and tantalum oxynitride[43] have been supported on graphitic carbon materials such as carbon black, carbon fibers, carbon nanotubes, and stacked graphene sheets via various routes, and the activities of these nanocatalysts have been evaluated in half-cells. However, single-cell performances were reported only for carbon black-supported zirconium oxynitride,[29] other examples being carbon-supported titanium nitride[44] and carbon-support-free titanium oxynitride.[45] The U.S. Department of Energy (DOE) set the activity target for non-PGM catalysts to be used in automotive PEFCs as 44 mA cm^{-2} at 0.9 V of Ohmic loss-free (IR-corrected) cell voltage.[46] Although the cell performances reported in refs 29 44, and 45 correspond to materials with nonoptimized layer structures, the first two catalysts showed open circuit voltages of less than 0.9 V,[29,44] with only the last catalyst showing a current density of 1 mA cm^{-2} at 0.9 V,[45] which is still lower than the value exhibited by a state-of-the-art Fe/N/C catalyst, 24 mA cm^{-2}.[46] The relatively low single-cell performance and the insulating nature of oxides/oxynitrides questioned the feasibility of their use in automotive PEFC cathodes because of the large currents involved.

Herein, we demonstrate both half- and single-cell activities of zirconium oxynitride (ZrO_xN_y) catalysts. Thermal decomposition of oxy-zirconium phthalocyanine (ZrOPc) in the presence of multiwalled carbon nanotube (MWCNT) supports was used to connect ZrO_xN_y nanoparticles to the above supports, followed by pyrolysis in an atmosphere of gaseous NH_3. The thus obtained ZrO_xN_y–MWCNT catalysts displayed the highest single-cell performance among oxide/oxynitride catalysts.

2. RESULTS AND DISCUSSION

Field emission transmission electron microscopy (FE-TEM) imaging of ZrO_xN_y–MWCNTs after pyrolysis in an atmosphere of NH_3 at 973 K (Figure 1a) shows that the black nanometer-sized ZrO_xN_y particles are well-dispersed in light-gray MWCNTs; however, some particles form aggregates on the order of several tens of nanometers in size. Furthermore, these ZrO_xN_y particles were also located on the amorphous carbon layer originating from ZrOPc (Figure S1), indicating that a modification of the synthetic route is necessary to produce size-uniform ZrO_xN_y nanoparticles on MWCNTs. Figure 1b reveals that these particles feature a single tetragonal ZrO_2 phase. Bulk ZrO_2 exists as a stable monoclinic phase under ambient conditions, transforming into a tetragonal phase at ∼1300 K[47] and into a cubic phase at ∼2600 K.[48] These phase transitions are reversible, and therefore, the monoclinic phase is stable after quenching to room temperature, that is, under the conditions of X-ray diffraction (XRD) pattern acquisition.

DOI: 10.1021/acsomega.6b00555
ACS Omega 2017, 2, 678−684

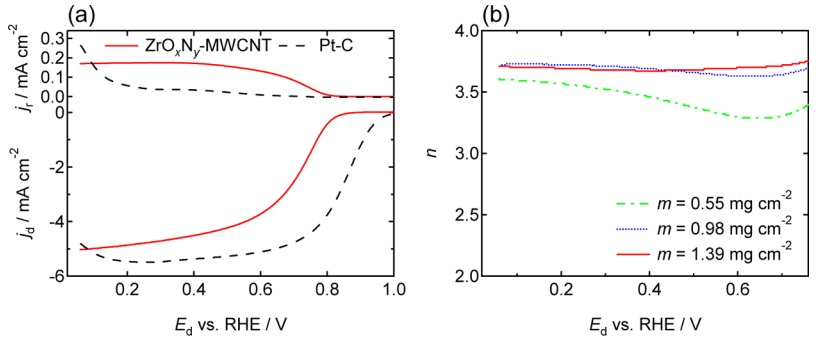

Figure 2. (a) RRDE voltammograms of ZrO_xN_y–MWCNTs and commercial Pt–C (50.8% Pt, w/w) catalysts and (b) n–E_d curves for ZrO_xN_y–MWCNTs with three different loadings (m). In (a), the values of m for ZrO_xN_y–MWCNTs and Pt–C equal 1.39 and 0.04 mg cm^{-2}, respectively, and the corresponding ZrO_xN_y loading of ZrO_xN_y–MWCNTs and the Pt loading of Pt–C equal 0.96 and 0.02 mg cm^{-2}, respectively. The optimized conditions of NH_3 pyrolysis used for the synthesis of ZrO_xN_y–MWCNTs corresponded to T = 973 K and t = 6 h. Scans were performed under N_2 and O_2 at a rotation speed of 1600 rpm and a disk potential (E_d) scan rate of −5 mV s^{-1} (cathodic) in 0.1 mol dm^{-3} H_2SO_4 for ZrO_xN_y–MWCNTs and 5 mV s^{-1} (anodic) in 0.1 mol dm^{-3} $HClO_4$ for Pt–C. The ring potential (E_r) was kept at 1.2 V. Both geometrical disk and ring current densities (j_d and j_r, respectively) were background-corrected.

However, tetragonal and cubic phases can be stabilized for nonbulk ZrO_2, that is, for grain sizes of less than ∼100 nm and/or grains containing inherent defects.[49] The small size of ZrO_xN_y particles shown in Figure 1a and/or the oxygen defects formed during NH_3 pyrolysis are therefore responsible for the stabilization of tetragonal ZrO_2. Further, rhombohedral $Zr_7O_8N_4$ formed when the temperature was increased to 1073–1173 K, transforming into cubic Zr_2ON_2 at 1273 K (Figure S2), which implies that nitrogen atoms were doped into the bulk at T > 973 K. NH_3 pyrolysis at 973 K did not significantly affect the surface chemical states, as shown by X-ray photoelectron Zr 3d and N 1s spectra in Figure 1c. The Zr 3d signal of the 973 K sample was split into Zr $3d_{5/2}$ and $3d_{3/2}$ peaks by spin–orbit coupling, appearing as a doublet at 182.6 and 184.9 eV assigned to Zr^{4+} in ZrO_2.[50−52] Compared to the signals observed before NH_3 pyrolysis (dashed line), these peaks were slightly shifted to lower binding energies, suggesting that the surface was partially reduced by NH_3 pyrolysis at 973 K. Both samples showed noisy N 1s spectra, with peaks above 398 eV attributed to zirconium oxynitride[50−53] and nitrogen-doped carbon species.[54] Because of a high degree of overlap, these peaks could not be deconvoluted; however, it can be concluded that NH_3 pyrolysis at 973 K did not significantly enhance the level of ZrO_2 surface nitrogen doping. If ZrO_2 powders are significantly doped with nitrogen, the Zr 3d peak shifts lower further by ∼0.5 eV and a new peak at around 396 eV appears in the N 1s spectrum (Figure S3). These reference sample data also indicate that the amount of nitrogen on the ZrO_2 surface of the 973 K sample is low. Similarly, the surfaces of MWCNTs and ZrO_2 were not significantly doped with the nitrogen atoms of ZrOPc during the first pyrolysis in the presence of 0.05% O_2. The surfaces of both polycrystalline zirconium[55] and zirconium oxynitride[51] are known to favor oxygen adsorption and form oxide layers, which could also happen in the case of ZrO_xN_y particles studied herein.

The temperature and duration of NH_3 pyrolysis were systematically optimized for ORR activity (Figure S4). Figure 2a shows rotating ring-disk electrode (RRDE) voltammograms of the most active ZrO_xN_y–MWCNT catalyst, the 973 K sample, and commercial Pt–C. The ZrO_xN_y–MWCNT composite exhibited high activity, displaying an overpotential of only 0.14 V higher than that of Pt–C. However, the ring current density (j_r) of ZrO_xN_y–MWCNTs was more than twice as high as that of Pt–C, indicating that the ORR proceeded via both two- ($O_2 + 2H^+ + 2e^- \rightarrow H_2O_2$) and four-electron pathways ($O_2 + 4H^+ + 4e^- \rightarrow 2H_2O$). To investigate the mechanism of ORR at ZrO_xN_y–MWCNTs in detail, RRDE voltammograms were recorded for three different loadings (m) to calculate n, the number of electrons transferred per oxygen molecule (see Experimental Section), as shown in Figure 2b. The value of n increased with increasing m, suggesting that some H_2O_2 molecules produced on the catalyst layer near the GC electrode side were further electrochemically reduced to water ($H_2O_2 + 2H^+ + 2e^- \rightarrow 2H_2O$) or chemically decomposed ($H_2O_2 \rightarrow H_2O + 0.5O_2$) before passing through the thicker catalyst layers to be detected at the ring electrode. During the synthesis of ZrO_xN_y–MWCNTs by NH_3 pyrolysis at 973 K, a small amount of nitrogen atoms were doped into both tetragonal ZrO_2 and carbon species originating from ZrOPc precursors and MWCNTs. To clarify the active sites of two- and four-electron pathways, ZrO_xN_y particles were completely removed by treatment with hydrofluoric (HF) acid (Figure S5). The resulting activity did not reach the original one, and the ORR proceeded mostly via the two-electron pathway on the ZrO_xN_y-free samples (Figure S5), indicating that the activity at disk potentials (E_d) above 0.8 V was due to ZrO_xN_y particles, and nitrogen-doped carbon species in ZrO_xN_y–MWCNTs produced H_2O_2 at a lower E_d. The activity of TaO_xN_y–MWCNTs was lower than that of ZrO_xN_y–MWCNTs at all temperatures T and times t (see Figure S4 and related discussions), supporting the hypothesis that oxynitrides determine the activity at a high E_d. Although the iron contaminants were not detected by X-ray photoelectron Fe 2p spectra (Figure S5), the presence of type-1 active sites on Fe/N/C, the so-called Fe–N_x sites, is not completely ruled out because some iron impurity is present in our catalyst precursors, especially in MWCNTs. However, all state-of-the-art Fe(Co)/N/C catalysts which exhibit a high ORR activity close to that of Pt–C were synthesized from the precursor mixture that was prepared by adding a non-negligible amount of iron salts.[4−10] Nitrogen-doped carbon species synthesized without adding iron/cobalt salts are known to catalyze the ORR via a two-electron pathway,[56−58] in line with the present results for ZrO_xN_y–MWCNTs. Furthermore, we also reported that nitrogen-doped carbon black produced by NH_3 pyrolysis catalyzes the formation of H_2O_2.[59] Therefore,

DOI: 10.1021/acsomega.6b00555
ACS Omega 2017, 2, 678–684

the selectivity for four-electron reduction can be enhanced by the use of carbon-free oxynitride catalysts.

The activity of ZrO_xN_y−MWCNTs was further evaluated for a single-cell cathode, with the voltage versus current density (V−j) curve shown in Figure 3. As mentioned earlier, most

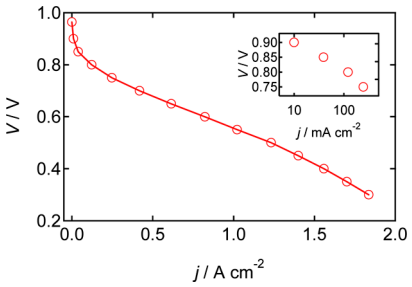

Figure 3. Cell voltage vs current density (V−j) curve for a membrane electrode assembly fabricated using a ZrO_xN_y−MWCNT (m = 10 mg cm^{-2}) cathode and a Pt−C anode (0.6 mg cm^{-2}, corresponding to a Pt loading of 0.3 mg cm^{-2}).

oxide-based catalysts exhibit no single-cell activity at V = 0.9 V, where DOE set the target current density, with only the titanium oxynitride catalyst showing an activity of 1 mA cm^{-2}.[45] The performance displayed by the present ZrO_xN_y−MWCNT composite is the highest ever reported for an oxide-based catalyst, with j = 10 mA cm^{-2} at V = 0.9 V without IR-correction. The corresponding open circuit voltage and the maximum power density equals 0.96 V and 0.63 W cm^{-2} at V = 0.45 V, respectively, being comparable to those of state-of-the-art Fe/N/C catalysts.[60] The stability of ZrO_xN_y−MWCNTs in a single-cell cathode, however, needs to be significantly improved (Figure S6); this issue is also similar to Fe/N/C catalysts.[60,61] Nonetheless, such a high performance has never been reported for iron-free oxide-based catalysts before, and the obtained results clearly show that catalysts of this type, for example, ZrO_xN_y, are suitable ORR catalysts for real PEFC cathodes.

3. CONCLUSIONS

In summary, ZrO_xN_y particles were supported on MWCNTs using thermal decomposition of ZrOPc at 1173 K under a flow of mixed $H_2/O_2/N_2$ gas. Subsequent pyrolysis in an atmosphere of NH_3 at 973 K produced highly ORR-active sites on ZrO_xN_y particles, with the corresponding overpotential being only 0.14 V higher than that observed for Pt−C in half-cells with acidic solutions. ZrO_xN_y also catalyzed the ORR on single-cell cathodes, exhibiting the highest performance ever reported for oxide-based catalysts.

4. EXPERIMENTAL SECTION

4.1. Catalyst Synthesis. ZrO_xN_y−MWCNT catalysts were synthesized by depositing ZrOPc on MWCNTs, followed by two-step pyrolysis. ZrOPc powder (1.2 g; Dainichi Seika Chemical Mfg. Co., Ltd., Chuo-ku, Tokyo, Japan) and MWCNT powder (0.3 g; Showa Denko K. K., Minato-ku, Tokyo, Japan) were dispersed in N-methylpyrrolidone (300 cm^3) using a homogenizer (Smurt NR-600M, Microtec Co., Ltd., Funabashi, Chiba, Japan) for 600 s and subsequently dried at 403 K in a vacuum oven. The obtained precursor mixture was placed in a rotary quartz-tube furnace that was slowly evacuated and purged with N_2 gas. The precursors were heated from room temperature to 1173 K at 20 K min^{-1} under a nitrogen gas flow of 50 standard cubic centimeters per minute (sccm; 1 sccm = 1.67 × 10^{-8} m^3 s^{-1}). After a temperature of 1173 K was reached, N_2 was replaced by a mixed gas containing 2% H_2, 0.05% O_2, and 97.95% N_2, and the above temperature was maintained for 7 h. The mixed gas was prepared using H_2/N_2 (4% H_2) and O_2/N_2 (0.1% O_2) mixtures, the flow rates of both being 50 sccm. After 7 h of pyrolysis, the gas was again switched to N_2 until reaching room temperature at an uncontrolled rate. The obtained powders were placed in an alumina boat and placed in a horizontal quartz-tube furnace, which was slowly evacuated and purged with N_2 gas. The powder samples were heated from room temperature to various temperatures T at a rate of 10 K min^{-1}, kept at T for various time intervals t, and cooled to room temperature at an uncontrolled rate. N_2 (300 sccm) and NH_3 (100 sccm) gas flows were used for temperatures below and equal to T, respectively. Unless otherwise noted, t = 6 h was used. To reveal the source of active sites, ZrO_xN_y particles were removed from ZrO_xN_y−MWCNTs exhibiting the highest activity (obtained after NH_3 pyrolysis at T = 973 K and t = 6 h) by treatment with HF acid at 353 K for 180 min, and the catalyst samples were recovered by filtration. The above treatment was repeated twice, and some HF-treated samples were further heated under Ar gas under conditions identical to those used for the first pyrolysis.

4.2. Physicochemical Characterization. The morphology of ZrO_xN_y−MWCNT catalysts was investigated using a field emission transmission electron microscope (TecnaiG2 F20, FEI Co., Minato-ku, Tokyo, Japan), and their crystal structures were analyzed using an X-ray diffractometer (XRD-6000, Shimadzu Co., Chukyo-ku, Kyoto, Japan; Cu K_α radiation generated at 40 kV and 30 mA) for a scan range of 15°−85° at a scan rate of 2° min^{-1}. The surface chemical states of catalysts were analyzed using an X-ray photoelectron spectrometer (PHI 5000 VersaProbe, ULVAC-PHI, Inc., Chigasaki, Kanagawa, Japan) with an Al K_α X-ray source (1486.6 eV). Peak shifts due to surface charge were corrected using the binding energy of C 1s at 284.8 eV.

4.3. Electrochemical Characterization. The catalyst ORR activities were evaluated by obtaining cyclic voltammograms (CVs). Catalyst powder (30 mg), an ultrapure water/isopropanol mixture (1.5 cm^3, 1:1 w/w), and 0.5% Nafion solution (50 mm^3, prepared by diluting a 5% (w/w) Nafion solution with ultrapure water) were sonicated for 600 s. The obtained catalyst slurry was drop-cast onto a GC rod (5.2 mm diameter, Tokai Carbon Co., Minato-ku, Tokyo, Japan) and dried. The mass of the catalyst coated on the GC rod was determined by measuring the rod mass before and after the coating procedure. The ORR selectivity of the best catalyst was evaluated by analyzing the RRDE voltammograms. An aliquot of the catalyst ink prepared using 1-hexanol as the solvent was drop-cast onto a GC disk (6 mm diameter)−platinum ring (7 mm inner diameter and 9 mm outer diameter) electrode (Nikko Keisoku, Atsugi, Kanagawa, Japan). Various catalyst loadings (m) were used to evaluate the ORR mechanism at a constant Nafion to catalyst ratio (0.1).

Electrochemical measurements were taken using a three-electrode cell in oxygen- or nitrogen-saturated 0.1 mol dm^{-3} H_2SO_4 at 303 K. The catalyst-coated GC rod or GC disk−ring electrode, a GC plate, and an RHE were used as working, counter, and reference electrodes, respectively. A potentiostat (PS08, TOHO Technical Research, Aoba-ku, Yokohama, Japan) and a bipotentiostat (CH Instruments, Inc., ALS

DOI: 10.1021/acsomega.6b00555
ACS Omega 2017, 2, 678−684

Model701C, Austin, TX, USA) were used to clean the working electrode surface by repeated scans from 0.05 to 1.2 V under oxygen at a rate of 150 mV s^{-1} for 150−400 cycles to reach a steady state. After cleaning, CVs were recorded from 1.2 to 0.05 V at a scan rate of 5 mV s^{-1} under oxygen and nitrogen. RRDE voltammograms were recorded using an identical disk potential (E_d) range and scan rate at a constant ring potential of 1.2 V and a rotation speed of 1600 revolutions per minute (rpm). Under both oxygen and nitrogen, the steady state was reached within three cycles, and therefore, data collected from the third cycle were used for the evaluation of ORR activity. The difference in the geometric current densities obtained under nitrogen (j_N) and oxygen (j_O) per unit mass of catalyst was taken as a measure of ORR activity, $j_M = (j_O - j_N)m^{-1}$. The number of electrons transferred per unit oxygen molecule (n) was calculated as follows

$$n = -4I_d/(-I_d + I_r/N) \quad (1)$$

where I_d and I_r denote the disk and ring currents, respectively, after the background correction described above, and N is the collection efficiency (0.381) determined by the reduction and oxidation of ferrocyanide ions at the disk and ring electrodes, respectively, using 0.1 M KNO_3 solution containing 2.1 mM $K_3[Fe(CN)_6]$. As a reference, RRDE voltammograms of a commercial carbon-supported platinum (Pt−C) catalyst (50.8% w/w platinum on Ketjen black, TEC10E50E, Tanaka Kikinzoku Kogyo K. K., Chiyoda-ku, Tokyo, Japan) were recorded under identical conditions, except for the scan direction and electrolyte, from 0.05 to 1.2 V (anodic) and 0.1 mol dm^{-3} $HClO_4$ because (bi)sulfate adsorption on platinum catalysts is known to block the initial adsorption of O_2 to decrease the activity.[62]

4.4. Single-Cell Tests. Inks for cathode catalyst layers were prepared using the ZrO_xN_y−MWCNT catalyst showing the highest level of activity (T = 973 K, t = 3 h), Ketjen black, 5% (w/w) Nafion ionomer solution, water, and n-propanol at a ZrO_xN_y−MWCNTs/Nafion ionomer/Ketjen black mass ratio of 9:6:1. First, ZrO_xN_y−MWCNT and Ketjen black were mixed at the mass ratio of 9:1 without a solvent using a zirconia planetary ball mill with 45 cm^3 of a grinding bowl and 90 balls of 5 mm diameter to achieve suitable conductivity. After the dry ball milling at 120 rpm for 60 min, 5% (w/w) Nafion ionomer solution and a solvent were added to the solid mixture. The solvent was prepared by blending water and n-propanol at water/n-propanol volume ratio of 1:1, and the amount was controlled to achieve the solid content in the ink to 10−12% (w/w). The second wet ball milling was conducted at 180 rpm for 60 min. Inks for anode catalyst layers were prepared from commercial Pt−C (TEC10E50E, Tanaka Kikinzoku Kogyo K. K., Chiyoda-ku, Tokyo, Japan), 20% (w/w) Nafion ionomer solution, water, and n-propanol. Cathode inks were coated on the gas-diffusion layer (Sigracet 35 BC, SGL Carbon Japan Co., Minato-ku, Tokyo, Japan) and dried in an oven at 343 K. The catalyst-coated gas-diffusion layers were hot-pressed onto one side of a Nafion membrane (NR-211, DuPont Co., Wilmington, DE, USA), whereas the anode catalyst layers were prepared on the opposite side by a decal transfer method. Following hot-pressing, the resultant membrane electrode assembly (MEA) was allowed to cool to room temperature. The Pt−C loading at the anode equaled 0.6 mg cm^{-2}, whereas the ZrO_xN_y−MWCNT loading at the cathode equaled 10 mg cm^{-2}.

The V−j curves for a single cell with the fabricated MEA were recorded galvanostatically using an electronic load (As-510-4, NF Corp., Yokohama, Kanagawa, Japan). All measurements were performed at 353 K. The H_2 and O_2 reactant gases were humidified by passing through separate water baths at 353 K. The flow rate of both H_2 and O_2 was 500 sccm, with back pressures (gage) of 0.2 and 0.3 MPa used for the anode and cathode, respectively. Stability of ZrO_xN_y−MWCNTs was further investigated using another MEA with two different protocols: one is a simple stability test with a constant j at 0.1 A cm^{-2} for 2 weeks and the other is an accelerated degradation test (ADT) in a load cycle mode proposed by Fuel Cell Commercialization Conference of Japan (FCCJ).[63] The ADT protocol is as follows: V was first set at 0.6 V (load) for 30 s. After the initial holding at 0.6 V, V was switched to 1.0 V (idle) immediately and kept for 3 s, then again switched to 0.6 V (load), and kept for 3 s. The rectangular wave-voltage cycle was repeated until it reached the cycle number, N, of 10 000 under conditions identical to those used for V−j measurements except for the following two parameters: (i) the cathode gas was N_2 at a flow rate of 500 sccm and (ii) both anode and cathode gases were supplied without back pressure. The cycle was stopped when N reached 10, 20, 30, 50, 100, 200, 300, 500, 1000, 2000, 3000, 5000, and 10 000; then, the cathode gas was switched to O_2 to obtain V−j curves with the back pressures as mentioned earlier.

■ ASSOCIATED CONTENT

Supporting Information

The Supporting Information is available free of charge on the ACS Publications website at DOI: 10.1021/acsomega.6b00555.

TEM images of ZrO_xN_y−MWCNTs, XRD patterns of MWCNTs and ZrO_xN_y−MWCNTs, XRD pattern and X-ray photoelectron spectra of of ZrO_xN_y powders, optimization of pyrolysis conditions for ORR activity, effect of HF treatment and the following pyrolysis on the activity and chemical states of ZrO_xN_y−MWCNTs, and stability of ZrO_xN_y−MWCNTs in a single cell (PDF)

■ AUTHOR INFORMATION

Corresponding Author

*E-mail: chisaka@hirosaki-u.ac.jp. Phone/Fax: +81 172 39 3559 (M.C.).

ORCID

Mitsuharu Chisaka: 0000-0002-9394-200X

Notes

The authors declare no competing financial interest.

■ ACKNOWLEDGMENTS

The authors gratefully acknowledge Dainichiseika Color & Chemicals Mfg. Co. and Showa Denko K. K. for supplying ZrOPc/TaOPc and MWCNT powders, respectively. This work was supported by the Japanese New Energy and Industrial Technology Development Organization (NEDO). X-ray photoelectron spectra were acquired with the support of the Nanotechnology Platform of the Ministry of Education, Culture, Sports, Science, and Technology (MEXT) of Japan.

■ REFERENCES

(1) Jaouen, F.; Herranz, J.; Lefèvre, M.; Dodelet, J.-P.; Kramm, U. I.; Herrmann, I.; Bogdanoff, P.; Maruyama, J.; Nagaoka, T.; Garsuch, A.; Dahn, J. R.; Olson, T.; Pylypenko, S.; Atanassov, P.; Ustinov, E. A.

DOI: 10.1021/acsomega.6b00555
ACS Omega 2017, 2, 678−684

Cross-Laboratory Experimental Study of Non-Noble-Metal Electrocatalysts for the Oxygen Reduction Reaction. *ACS Appl. Mater. Interfaces* **2009**, *1*, 1623.
(2) Yoshida, T.; Kojima, K. Toyota MIRAI Fuel Cell Vehicle and Progress toward a Future Hydrogen Society. *Electrochem. Soc. Interface* **2015**, *24*, 45.
(3) Dodelet, J. P. *Electrocatalysis in Fuel Cells*; Shao, M., Ed.; Springer, 2013; p 271.
(4) Proietti, E.; Jaouen, F.; Lefèvre, M.; Larouche, N.; Tian, J.; Herranz, J.; Dodelet, J.-P. Iron-Based Cathode Catalyst with Enhanced Power Density in Polymer Electrolyte Membrane Fuel Cells. *Nat. Commun.* **2011**, *2*, 416.
(5) Singh, D.; Tian, J.; Mamtani, K.; King, J.; Miller, J. T.; Ozkan, U. S. A Comparison of N-Containing Carbon Nanostructures (CN_x) and N-coordinated Iron−Carbon Catalysts (FeNC) for the Oxygen Reduction Reaction in Acidic Media. *J. Catal.* **2014**, *317*, 30.
(6) Serov, A.; Artyushkova, K.; Atanassov, P. Fe−N−C Oxygen Reduction Fuel Cell Catalyst Derived from Carbendazim: Synthesis, Structure, and Reactivity. *Adv. Energy Mater.* **2014**, *4*, 1301735.
(7) Shui, J.; Chen, C.; Grabstanowicz, L.; Zhao, D.; Liu, D.-J. Highly Efficient Nonprecious Metal Catalyst Prepared with Metal−Organic Framework in a Continuous Carbon Nanofibrous Network. *Proc. Natl. Acad. Sci. U.S.A.* **2015**, *112*, 10629.
(8) Wang, Y.-C.; Lai, Y.-J.; Song, L.; Zhou, Z.-Y.; Liu, J.-G.; Wang, Q.; Yang, X.-D.; Chen, C.; Shi, W.; Zheng, Y.-P.; Rauf, M.; Sun, S.-G. S-Doping of an Fe/N/C ORR Catalyst for Polymer Electrolyte Membrane Fuel Cells with High Power Density. *Angew. Chem., Int. Ed.* **2015**, *54*, 9907.
(9) Zitolo, A.; Goellner, V.; Armel, V.; Sougrati, M.-T.; Mineva, T.; Stievano, L.; Fonda, E.; Jaouen, F. Identification of Catalytic Sites for Oxygen Reduction in Iron- and Nitrogen-Doped Graphene Materials. *Nat. Mater.* **2015**, *14*, 937.
(10) Nabae, Y.; Nagata, S.; Hayakawa, T.; Niwa, H.; Harada, Y.; Oshima, M.; Isoda, A.; Matsunaga, A.; Tanaka, K.; Aoki, T. Pt-Free Carbon-Based Fuel Cell Catalyst Prepared from Spherical Polyimide for Enhanced Oxygen Diffusion. *Sci. Rep.* **2016**, *6*, 23276.
(11) Liu, G.; Li, X.; Ganesan, P.; Popov, B. N. Development of Non-Precious Metal Oxygen-Reduction Catalysts for PEM Fuel Cells Based on N-Doped Ordered Porous Carbon. *Appl. Catal., B* **2009**, *93*, 156.
(12) Shui, J.; Wang, M.; Du, F.; Dai, L. N-Doped Carbon Nanomaterials are Durable Catalysts for Oxygen Reduction Reaction in Acidic Fuel Cells. *Sci. Adv.* **2015**, *1*, No. e1400129.
(13) Hu, Y.; Jensen, J. O.; Zhang, W.; Cleemann, L. N.; Xing, W.; Bjerrum, N. J.; Li, Q. Hollow Spheres of Iron Carbide Nanoparticles Encased in Graphitic Layers as Oxygen Reduction Catalysts. *Angew. Chem., Int. Ed.* **2014**, *53*, 3675.
(14) Varnell, J. A.; Tse, E. C. M.; Schulz, C. E.; Fister, T. T.; Haasch, R. T.; Timoshenko, J.; Frenkel, A. I.; Gewirth, A. A. Identification of Carbon-Encapsulated Iron Nanoparticles as Active Species in Non-Precious Metal Oxygen Reduction Catalysts. *Nat. Commun.* **2016**, *7*, 12582.
(15) Doi, S.; Ishihara, A.; Mitsushima, S.; Kamiya, N.; Ota, K.-i. Zirconium-Based Compounds for Cathode of Polymer Electrolyte Fuel Cell. *J. Electrochem. Soc.* **2007**, *154*, B362.
(16) Shibata, Y.; Ishihara, A.; Mitsushima, S.; Kamiya, N.; Ota, K. Effect of Heat Treatment on Catalytic Activity for Oxygen Reduction Reaction of TaO_xN_y/Ti Prepared by Electrophoretic Deposition. *Electrochem. Solid-State Lett.* **2007**, *10*, B43.
(17) Kim, J.-H.; Ishihara, A.; Mitsushima, S.; Kamiya, N.; Ota, K.-i. Catalytic Activity of Titanium Oxide for Oxygen Reduction Reaction as a Non-Platinum Catalyst for PEFC. *Electrochim. Acta* **2007**, *52*, 2492.
(18) Ishihara, A.; Doi, S.; Mitsushima, S.; Ota, K.-i. Tantalum (Oxy)Nitrides Prepared Using Reactive Sputtering for New Non-platinum Cathodes of Polymer Electrolyte Fuel Cell. *Electrochim. Acta* **2008**, *53*, 5442.
(19) Chisaka, M.; Iijima, T.; Yaguchi, T.; Sakurai, Y. Carbon-Supported Hafnium Oxynitride as Cathode Catalyst for Polymer Electrolyte Membrane Fuel Cells. *Electrochim. Acta* **2011**, *56*, 4581.
(20) Jasinski, R. A New Fuel Cell Cathode Catalyst. *Nature* **1964**, *201*, 1212.
(21) Ukita, K.; Ishihara, A.; Ohgi, Y.; Matsuzawa, K.; Mitsushima, S.; Ota, K.-i. Zirconium Oxide-Based Compounds as Non-Pt Cathode for Polymer Electrolyte Fuel Cell. *Electrochemistry* **2011**, *79*, 340.
(22) Chisaka, M.; Ishihara, A.; Ota, K.-i.; Muramoto, H. Synthesis of Carbon-Supported Titanium Oxynitride Nanoparticles as Cathode Catalyst for Polymer Electrolyte Fuel Cells. *Electrochim. Acta* **2013**, *113*, 735.
(23) Chisaka, M.; Muramoto, H. Reduced Graphene-Oxide-Supported Titanium Oxynitride as Oxygen Reduction Reaction Catalyst in Acid Media. *ChemElectroChem* **2014**, *1*, 544.
(24) Chisaka, M.; Ando, Y.; Muramoto, H. Facile Combustion Synthesis of Carbon-Supported Titanium Oxynitride to Catalyse Oxygen Reduction Reaction in Acidic Media. *Electrochim. Acta* **2015**, *183*, 100.
(25) Kinumoto, T.; Sou, Y.; Ono, K.; Matsuoka, M.; Arai, Y.; Tsumura, T.; Toyoda, M. Preparation of Fibrous Titania Oxynitride−Carbon Catalyst and Oxygen Reduction Reaction Analysis in both Acidic and Alkaline Media. *J. Power Sources* **2015**, *273*, 136.
(26) Chisaka, M.; Ando, Y.; Itagaki, N. Activity and Durability of the Oxygen Reduction Reaction in a Nitrogen-Doped Rutile-Shell on TiN-Core Nanocatalysts Synthesised via Solution-Phase Combustion. *J. Mater. Chem. A* **2016**, *4*, 2501.
(27) Seo, J.; Cha, D.; Takanabe, K.; Kubota, J.; Domen, K. Electrodeposited Ultrafine NbO_x, ZrO_x, and TaO_x Nanoparticles on Carbon Black Supports for Oxygen Reduction Electrocatalysts in Acidic Media. *ACS Catal.* **2013**, *3*, 2181.
(28) Okada, Y.; Ishihara, A.; Matsumoto, M.; Arao, M.; Imai, H.; Kohno, Y.; Matsuzawa, K.; Mitsushima, S.; Ota, K. Effect of Reheating Treatment on Oxygen-Reduction Activity and Stability of Zirconium Oxide-Based Electrocatalysts Prepared from Oxy-Zirconium Phthalocyanine for Polymer Electrolyte Fuel Cells. *J. Electrochem. Soc.* **2015**, *162*, F959.
(29) Liu, G.; Zhang, H. M.; Wang, M. R.; Zhong, H. X.; Chen, J. Preparation, Characterization of ZrO_xN_y/C and its Application in PEMFC as an Electrocatalyst for Oxygen Reduction. *J. Power Sources* **2007**, *172*, 503.
(30) Ohnishi, R.; Katayama, M.; Takanabe, K.; Kubota, J.; Domen, K. Niobium-based Catalysts Prepared by Reactive Radio-frequency Magnetron Sputtering and Arc Plasma Methods as Non-Noble Metal Cathode Catalysts for Polymer Electrolyte Fuel Cells. *Electrochim. Acta* **2010**, *55*, 5393.
(31) Takagaki, A.; Takahashi, Y.; Yin, F.; Takanabe, K.; Kubota, J.; Domen, K. Highly Dispersed Niobium Catalyst on Carbon Black by Polymerized Complex Method as PEFC Cathode Catalyst. *J. Electrochem. Soc.* **2009**, *156*, B811.
(32) Chisaka, M.; Itagaki, N. Evaluation and Enhancement of the Oxygen Reduction Reaction Activity on Hafnium Oxide Nanoparticles Assisted by L(+)-Lysine. *Electrochim. Acta* **2016**, *201*, 279.
(33) Chisaka, M.; Suzuki, Y.; Iijima, T.; Sakurai, Y. Effect of Synthesis Route on Oxygen Reduction Reaction Activity of Carbon-Supported Hafnium Oxynitride in Acid Media. *J. Phys. Chem. C* **2011**, *115*, 20610.
(34) Chisaka, M.; Suzuki, Y.; Iijima, T.; Ishihara, Y.; Inada, R.; Sakurai, Y. Active Sites for Oxygen Reduction Reaction and the Reaction Mechanism in Carbon-Supported Hafnium Oxynitride. *ECS Electrochem. Lett.* **2012**, *1*, F4.
(35) Chisaka, M.; Muramoto, H. Suppression and Evaluation of Hydrogen Peroxide Formation on Carbon-Supported Hafnium Oxynitride. *ECS Electrochem. Lett.* **2014**, *3*, F1.
(36) Chisaka, M.; Sasaki, H.; Muramoto, H. Monoclinic Hafnium Oxynitride Supported on Reduced Graphene Oxide to Catalyse the Oxygen Reduction Reaction in Acidic Media. *Phys. Chem. Chem. Phys.* **2014**, *16*, 20415.
(37) Chisaka, M.; Muramoto, H. Aluminum-Doped Hafnium Oxynitride: Effect of Cation Doping on Oxygen-Reduction-Reaction Activity in Acid Media. *ChemElectroChem* **2014**, *1*, 863.

DOI: 10.1021/acsomega.6b00555
ACS Omega 2017, 2, 678−684

(38) Kim, J. Y.; Oh, T.-K.; Shin, Y.; Bonnett, J.; Weil, K. S. A Novel Non-Platinum Group Electrocatalyst for PEM Fuel Cell Application. *Int. J. Hydrogen Energy* **2011**, *36*, 4557.
(39) Seo, J.; Cha, D.; Takanabe, K.; Kubota, J.; Domen, K. Highly-Dispersed Ta-Oxide Catalysts Prepared by Electrodeposition in a Non-Aqueous Plating Bath for Polymer Electrolyte Fuel Cell Cathodes. *Chem. Commun.* **2012**, *48*, 9074.
(40) Seo, J.; Anjum, D. H.; Takanabe, K.; Kubota, J.; Domen, K. Electrodeposited Ultrafine TaO_x/CB Catalysts for PEFC Cathode Application: Their Oxygen Reduction Reaction Kinetics. *Electrochim. Acta* **2014**, *149*, 76.
(41) Ishihara, A.; Chisaka, M.; Ohgi, Y.; Matsuzawa, K.; Mitsushima, S.; Ota, K. Synthesis of Nano-TaO_x Oxygen Reduction Reaction Catalysts on Multi-Walled Carbon Nanotubes Connected via a Decomposition of Oxy-Tantalum Phthalocyanine. *Phys. Chem. Chem. Phys.* **2015**, *17*, 7643.
(42) Sebastián, D.; Baglio, V.; Sun, S.; Tavares, A. C.; Aricò, A. S. Graphene-Supported Substoichiometric Sodium Tantalate as a Methanol-Tolerant, Non-Noble-Metal Catalyst for the Electroreduction of Oxygen. *ChemCatChem* **2015**, *7*, 911.
(43) Chisaka, M.; Ishihara, A.; Uehara, N.; Matsumoto, M.; Imai, H.; Ota, K. Nano-TaO_xN_y Particles Synthesized from Oxy-Tantalum Phthalocyanine: How to Prepare Precursors to Enhance the Oxygen Reduction Reaction Activity after Ammonia Pyrolysis? *J. Mater. Chem. A* **2015**, *3*, 16414.
(44) Chen, J.; Takanabe, K.; Ohnishi, R.; Lu, D.; Okada, S.; Hatasawa, H.; Morioka, H.; Antonietti, M.; Kubota, J.; Domen, K. Nano-Sized TiN on Carbon Black as an Efficient Electrocatalyst for the Oxygen Reduction Reaction Prepared Using an mpg-C_3N_4 Template. *Chem. Commun.* **2010**, *46*, 7492.
(45) Chisaka, M.; Ando, Y.; Yamamoto, Y.; Itagaki, N. A Carbon-Support-Free Titanium Oxynitride Catalyst for Proton Exchange Membrane Fuel Cell Cathodes. *Electrochim. Acta* **2016**, *214*, 165.
(46) Fuel Cell Technologies Office Multi-Year Research, *Development, and Demonstration Plan*, 3.4 Fuel Cells; U.S. Department of Energy, 2016; p 3.4-21, http://energy.gov/sites/prod/files/2016/10/f33/fcto_myrdd_fuel_cells.pdf.
(47) Wolten, G. M. Diffusionless Phase Transformations in Zirconia and Hafnia. *J. Am. Ceram. Soc.* **1963**, *46*, 418.
(48) Smith, D. K.; Cline, C. F. Verification of Existence of Cubic Zirconia at High Temperature. *J. Am. Ceram. Soc.* **1962**, *45*, 249.
(49) Navrotsky, A. Thermochemical insights into refractory ceramic materials based on oxides with large tetravalent cations. *J. Mater. Chem.* **2005**, *15*, 1883.
(50) Wiame, H.; Centeno, M.-A.; Picard, S.; Bastians, P.; Grange, P. Thermal Oxidation under Oxygen of Zirconium Nitride Studied by XPS, DRIFTS, TG-MS. *J. Eur. Ceram. Soc.* **1998**, *18*, 1293.
(51) Carvalho, P.; Chappé, J. M.; Cunha, L.; Lanceros-Méndez, S.; Alpuim, P.; Vaz, F.; Alves, E.; Rousselot, C.; Espinós, J. P.; González-Elipe, A. R. Influence of the Chemical and Electronic Structure on the Electrical Behavior of Zirconium Oxynitride Films. *J. Appl. Phys.* **2008**, *103*, 104907.
(52) Rizzo, A.; Signore, M. A.; Mirenghi, L.; Luccio, T. D. Synthesis and Characterization of Titanium and Zirconium Oxynitride Coatings. *Thin Solid Films* **2009**, *517*, 5956.
(53) Cheng, C.-C.; Chien, C.-H.; Lin, J.-H.; Chang, C.-Y.; Luo, G.-L.; Yang, C.-H.; Hsu, S.-L. Thermochemical reaction of $ZrO_x(N_y)$ interfaces on Ge and Si substrates. *Appl. Phys. Lett.* **2006**, *89*, 012905.
(54) Pels, J. R.; Kapteijn, F.; Moulijn, J. A.; Zhu, Q.; Thomas, K. M. Evolution of Nitrogen Functionalities in Carbonaceous Materials During Pyrolysis. *Carbon* **1995**, *33*, 1641.
(55) Foord, J. S.; Goddard, P. J.; Lambert, R. M. Adsorption and Absorption of Diatomic Gases by Zirconium: Studies of the Dissociation and Diffusion of CO, NO, N_2, O_2 and D_2. *Sur. Sci.* **1980**, *94*, 339.
(56) Park, J.; Nabae, Y.; Hayakawa, T.; Kakimoto, M.-a. Highly Selective Two-Electron Oxygen Reduction Catalyzed by Mesoporous Nitrogen-Doped Carbon. *ACS Catal.* **2014**, *4*, 3749.
(57) Artyushkova, K.; Serov, A.; Rojas-Carbonell, S.; Atanassov, P. Chemistry of Multitudinous Active Sites for Oxygen Reduction Reaction in Transition Metal−Nitrogen−Carbon Electrocatalysts. *J. Phys. Chem. C* **2015**, *119*, 25917.
(58) Noffke, B. W.; Li, Q.; Raghavachari, K.; Li, L.-s. A Model for the pH-Dependent Selectivity of the Oxygen Reduction Reaction Electrocatalyzed by N-Doped Graphitic Carbon. *J. Am. Chem. Soc.* **2016**, *138*, 13923.
(59) Chisaka, M.; Muramoto, H. Suppression and Evaluation of Hydrogen Peroxide Formation on Carbon-Supported Hafnium Oxynitride. *ECS Electrochem. Lett.* **2014**, *3*, F1.
(60) Shao, M.; Chang, Q.; Dodelet, J.-P.; Chenitz, R. Recent Advances in Electrocatalysts for Oxygen Reduction Reaction. *Chem. Rev.* **2016**, *116*, 3594.
(61) Zhang, G.; Chenitz, R.; Lefèvre, M.; Sun, S.; Dodelet, J.-P. Is Iron Involved in the Lack of Stability of Fe/N/C Electrocatalysts Used to Reduce Oxygen at the Cathode of PEM Fuel Cells? *Nano Energy* **2016**, *29*, 111.
(62) Stamenković, V.; Schmidt, T. J.; Ross, P. N.; Marković, N. M. Surface Composition Effects in Electrocatalysis: Kinetics of Oxygen Reduction on Well-Defined Pt_3Ni and Pt_3Co Alloy Surfaces. *J. Phys. Chem. B* **2002**, *106*, 11970.
(63) Ohma, A.; Shinohara, K.; Iiyama, A.; Yoshida, T.; Daimaru, A. Membrane and Catalyst Performance Targets for Automotive Fuel Cells by FCCJ Membrane, Catalyst, MEA WG. *ECS Trans.* **2011**, *41*, 775.

DOI: 10.1021/acsomega.6b00555
ACS Omega 2017, 2, 678−684